THE JOURNAL OF PHYSICAL CHEMISTRY C

Article

pubs.acs.org/JPCC

CO_2 Conversion in a Microwave Plasma Reactor in the Presence of N_2: Elucidating the Role of Vibrational Levels

Stijn Heijkers,*[,†] Ramses Snoeckx,[†] Tomáš Kozák,[†,‡] Tiago Silva,[§] Thomas Godfroid,[∥] Nikolay Britun,[§] Rony Snyders,[§,∥] and Annemie Bogaerts*[,†]

[†]Research Group PLASMANT, Department of Chemistry, University of Antwerp, Universiteitsplein 1, BE-2610 Wilrijk-Antwerp, Belgium

[‡]Department of Physics and NTIS, European Centre of Excellence, University of West Bohemia, Univerzitní 8, 30614 Plzeň, Czech Republic

[§]Chimie des Interactions Plasma-Surface (ChIPS), CIRMAP, Université de Mons, 20 Place du Parc, B-7000 Mons, Belgium

[∥]Materia Nova Research Center, Parc Initialis, B-7000 Mons, Belgium

Supporting Information

ABSTRACT: A chemical kinetics model is developed for a CO_2/N_2 microwave plasma, focusing especially on the vibrational levels of both CO_2 and N_2. The model is used to calculate the CO_2 and N_2 conversion as well as the energy efficiency of CO_2 conversion for different power densities and for N_2 fractions in the CO_2/N_2 gas mixture ranging from 0 to 90%. The calculation results are compared with measurements, and agreements within 23% and 33% are generally found for the CO_2 conversion and N_2 conversion, respectively. To explain the observed trends, the destruction and formation processes of both CO_2 and N_2 are analyzed, as well as the vibrational distribution functions of both CO_2 and N_2. The results indicate that N_2 contributes in populating the lower asymmetric levels of CO_2, leading to a higher absolute CO_2 conversion upon increasing N_2 fraction. However, the effective CO_2 conversion drops because there is less CO_2 initially present in the gas mixture; thus, the energy efficiency also drops with rising N_2 fraction.

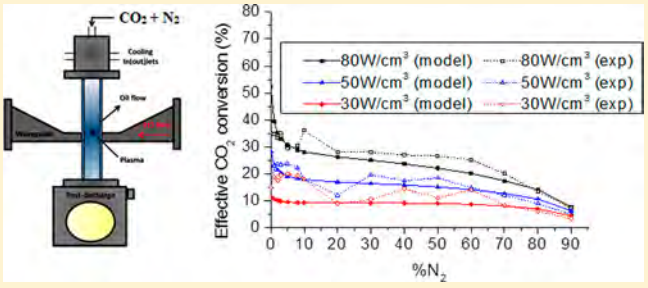

1. INTRODUCTION

In recent years, there has been considerable interest in the plasma-based conversion of CO_2 into value-added chemicals or fuels by means of different types of plasmas.[1−23] Microwave (MW) plasma is gaining increasing interest[5−12] because of the high energy efficiencies reported under some conditions.[1,13,14] Most experiments are carried out in pure CO_2[3−9] or in combination with CH_4 (i.e., dry reforming),[11,12,15−19] H_2,[20,21] H_2O,[10] or an inert gas.[22,23] However, in real gas emissions from combustion or the chemical industry, the CO_2 will not be in pure form, but will be mixed with other gases, such as N_2. It is therefore crucial to study the effect of N_2 on the CO_2 conversion and on the energy efficiency of the process. A few experiments have been performed for CO_2/N_2 mixtures, more specifically in a gliding arc[4] and a glow discharge.[24] In both cases, a higher CO_2 conversion was found when adding N_2. However, the exact mechanisms for the conversion of CO_2 and N_2 were not discussed, and to our knowledge, no experiments have been performed to date for CO_2/N_2 mixtures in a microwave discharge.

Computer modeling can be very useful in providing more insight into the underlying reaction mechanisms of the effect of N_2 on CO_2 conversion. The modeling of CO_2/N_2 plasmas was initially motivated by the application of CO_2 lasers.[25,26] However, these early models did not include the vibrational levels of the molecules, which are stated to be important in certain plasmas, especially in a microwave plasma, and for the application of CO_2 conversion.[1] For pure N_2, or N_2/O_2 mixtures, there are several papers presenting kinetic models with a complex description of vibrational and electronic levels (for example, see refs 27 and 28). The diatomic molecules are significantly easier to model than CO_2 because it is possible to include all (i.e., several tens of) vibrational levels of their single vibrational mode in a straightforward manner. Also, there are more reliable reaction rate coefficients available from various experiments and ab initio calculations. Nevertheless, the various mechanisms that contribute to the dissociation of N_2 in a microwave plasma seem not to be completely elucidated.[29]

For the dissociation of pure CO_2 in a plasma, Rusanov and Fridman presented a model combining a kinetic description of the chemical reactions and a temperature-based description of the vibrational distribution functions of CO_2 and CO.[1,13] On

Received: February 12, 2015
Revised: May 11, 2015
Published: May 13, 2015

DOI: 10.1021/acs.jpcc.5b01466
J. Phys. Chem. C 2015, 119, 12815−12828

the basis of their work, we have presented a reaction kinetics model for the dissociation of CO_2 in a MW plasma and a dielectric barrier discharge,[30,31] which includes state-to-state reactions of vibrational levels of CO_2 and CO in a manner similar to what was done for N_2 in the above-mentioned works. However, to our knowledge, there exist no models yet for a CO_2/N_2 plasma, including the vibrational levels.

In the present paper, we show the results of such a computer model developed for studying the effect of N_2 on the CO_2 conversion in a MW plasma, taking into account the vibrational levels of both CO_2 and N_2. Indeed, it is known that the CO_2 vibrational levels are very important for energy-efficient CO_2 conversion in a MW plasma.[1,30,31] Therefore, we will focus especially on the behavior of the CO_2 vibrational levels, how they are affected by the presence of N_2 (and their vibrational levels), and consequently how this influences the CO_2 conversion and energy efficiency in the MW plasma.

2. MODEL DESCRIPTION

The model used for this study is a zero-dimensional (0D) chemical kinetics model, called ZDPlaskin.[32] In this model, the time-evolution of the species densities is calculated by balance equations, taking into account the various production and loss terms by chemical reactions. Transport processes are not considered; hence, the species densities are assumed to be constant in the entire simulation volume. The rate coefficients of these reactions are assumed to be constant and are adopted from the literature for the heavy particle reactions, whereas the rate coefficients for the electron impact reactions are calculated with a Boltzmann solver, BOLSIG+,[33] which is integrated into ZDPlaskin. This Boltzmann routine uses the two-term approximation, which is less accurate than using multiterm Boltzmann routines.[34,35] Typically, the rate constants calculated using the two-term approximation show an error of approximately 30%.[36−38] Furthermore, the uncertainty in the rate constants of the most important neutral reactions (see section 4.3) is typically around 100%.[39−41] Therefore, we performed a sensitivity analysis to check whether variations of 30% in electron impact reaction rate constants and variations of 100% in neutral reaction rate constants have a significant effect on the CO_2 and N_2 conversion and on the vibrational kinetics (see Supporting Information). The results indicate that these variations do not affect the results to a large extent. More information about the model can be found in ref 32. In the following sections we will describe in a bit more detail the general reaction chemistry assumed in the model (section 2.1), with special emphasis on the vibrational levels (section 2.2), and we conclude with explaining how we apply this 0D model to a MW reactor (section 2.3).

2.1. General Reaction Chemistry. The species taken into account in our model for the CO_2/N_2 mixture are listed in Table 1. These species include various neutral molecules in the ground state as well as several electronic and vibrationally excited levels, various radicals, positive and negative ions, and the electrons. Besides the input gases (CO_2 and N_2), also various formed products are included, such as CO, O_2, O_3, several NO_x compounds, as well as some other CO_2-derived compounds, N−C and N−C−O compounds. CO_2(V) and CO_2(E) indicate the vibrational and electronic excited levels of CO_2. Because the asymmetric mode levels are most important for the splitting of CO_2,[1,42] all these levels up to the dissociation limit are included in the model (i.e., 21 levels), whereas only a few symmetric model levels are incorporated, following the example of the model developed by Kozák and Bogaerts.[30] Similarly, CO(V), CO(E), O_2(V), and O_2(E) indicate the vibrational and electronic excited levels of CO and O_2, which are sometimes composed of several individual levels. The detailed notation for these vibrational and electronic excited levels are summarized in Table 2.

Table 1. Overview of the Species Included in the Model

CO_2 compounds	CO_2, CO_2(Va), CO_2(Vb), CO_2(Vc), CO_2(Vd), CO_2(V1−V21), CO_2(E1), CO_2(E2), CO_2^+
derived CO_2 compounds	C_2O, $C_2O_2^+$, $C_2O_3^+$, $C_2O_4^+$, C_2, C_2^+, C, C^+
CO compounds	CO, CO(V1−V10), CO(E1), CO(E2), CO(E3), CO(E4), CO^+, CO_3^-, CO_4^-, CO_4^+
O_3, O_2 ,and O compounds	O_2, O_2(V1), O_2(V2), O_2(V3), O_2(V4), O_2(E1), O_2(E2), O_2^+, O_2^-, O, O^+, O^-, O_4^-, O_4^+, O_3, O_3^-
pure N compounds	N_2, N_2(V1−V14), $N_2(C^3\Pi_u)$, $N_2(A^3\Sigma_u^+)$, $N_2(a'^1\Sigma_u^-)$, $N_2(B^3\Pi_g)$, N^+, N_2^+, N_3^+, N_4^+, N, N(2D), N(2P)
N−O compounds	NO, N_2O, NO_2, NO_3, N_2O_5, NO^+, N_2O^+, NO_2^+, NO^-, N_2O^-, NO_2^-, NO_3^-, $N_2O_2^+$
N−O−C compounds and N−C compounds	CN, ONCN, NCO, C_2N_2, NCN
electrons	e^-

All these species undergo a large number of chemical reactions, like electron impact collisions with neutral species, leading to excitation, ionization, dissociation and electron-attachment, electron−ion recombination reactions, as well as many heavy-particle chemical reactions (i.e., between neutral species and/or ions).

The chemical reaction set described in this model is partly based on the model by Kozák and Bogaerts[30] (i.e., for the entire CO_2 chemistry, including the vibrational levels of CO_2, CO, and O_2) and the work of Pancheshnyi et al.[32] (for the N_2/O_2 chemistry); hence, all details of the reactions and the corresponding rate coefficients can be found in these references. The coupling reactions between CO_2 and N_2 and their reaction products, mostly in the ground state or electronically excited, were not included in the above chemistry sets and were therefore added in our work to complete the reaction set for the CO_2/N_2 mixture. These extra reactions, as well as the corresponding rate coefficients, are listed in the Supporting Information (Tables A1−A4). Note that the reactions or relaxation processes and their rate coefficients are tabulated for the ground state or lowest vibrational state, respectively. The same processes are also included for the higher vibrational levels, and the corresponding rate coefficients are calculated with the theories explained in section 2.2.

2.2. Description of the Vibrational Levels. Because the vibrationally excited species play an important role in the CO_2 conversion in a MW plasma, as mentioned above, we pay special attention to their kinetics. In the following sections, we therefore describe the different vibrational levels included in the model, as well as the methods to calculate their rate coefficients.

2.2.1. Vibrational Levels Taken into Account. CO_2 has three vibration modes: the symmetric stretch mode, the bending mode (which is double degenerate), and the asymmetric stretch mode. As mentioned above, the asymmetric stretch mode is most important for the CO_2 dissociation;[1,42] therefore, for this mode all levels up to the dissociation limit of 5.5 eV are taken into account, whereas only four effective vibrational levels of the symmetric modes are included, in the same way as was described by Kozák and Bogaerts; for details, we refer to ref 30.

DOI: 10.1021/acs.jpcc.5b01466
J. Phys. Chem. C 2015, 119, 12815−12828

Table 2. Explanation of the Notations for the Vibrational and Electronic Excited Levels of CO_2, CO, and O_2

CO_2 levels	CO levels	O_2 levels
$CO_2(Va) = (010)$	$CO(E1) = CO(A^3\Pi)$	$O_2(E1)$ = sum of the $A^1\Delta$ and $b^1\Sigma$ states
$CO_2(Vb) = (100), (020)$	$CO(E2) = CO(A^1\Pi)$	$O_2(E2) = O_2(B^3\Sigma)$ and higher triplet states
$CO_2(Vc) = (110), (030)$	$CO(E3) = CO(A^3\Sigma), CO(D^3\Delta), CO(E^3\Sigma), CO(B^3\Sigma)$	
$CO_2(Vd) = (040), (120), (200)$	$CO(E4) = CO(C^1\Sigma), CO(E^1\Pi), CO(B^1\Sigma), CO(I^1\Sigma), CO(D^1\Delta)$	
$XO_2(Vn) = (00n)$ with $n = 1\cdots21$		
$CO_2(E1) = CO_2(^1\Pi_g)$		
$CO_2(E2) = CO_2(^1\Delta_u)$		

For the diatomic molecules, i.e., CO, N_2, and O_2, the energies of the various vibrational levels are calculated as

$$\frac{E(\xi)}{hc} = \omega_e\xi - \omega_e x_e\xi^2 + \omega_e y_e\xi^3 + \omega_e z_e\xi^4 \quad (1)$$

In this equation, ω_e, $\omega_e x_e$, $\omega_e y_e$, and $\omega_e z_e$ are spectroscopic constants (in cm^{-1}) that are characteristic for the molecule and $\xi = (\upsilon + (1/2))$ with υ being the vibrational quantum number. The values of the spectroscopic constants are listed in Table 3.

Table 3. Spectroscopic Constants Used for Calculating the Energies of the Various Vibrational Levels of CO, N_2, and O_2

	CO	N_2	O_2
ω_e	2170.21	2372.45	1580.19
$\omega_e x_e$	13.46	18.1017	11.98
$\omega_e y_e$	0.0308	1.27552×10^{-2}	0.0474
$\omega_e z_e$	0.0	-7.95949×10^{-5}	-1.27×10^{-3}

Ten vibrational levels are taken into account for CO, and 4 levels for O_2, as in Kozák and Bogaerts.[30] For N_2, 14 vibrational levels are included because the populations of the higher levels are negligible, as will be demonstrated in section 4.5.

2.2.2. Processes of the Vibrational Levels Considered in the Model. 2.2.2.1. Vibrational Excitation. Electron impact vibrational excitation is very important for populating the lower vibrational levels. The rate coefficients of this process for the lower vibrational levels are calculated from the cross sections adopted from the LXCAT database. To obtain the cross sections for electron impact vibrational excitation to the higher vibrational levels, we use the Fridman approximation,[1] which is based on the following semiempirical formula:

$$\sigma_{nm}(\varepsilon) = \exp\left(\frac{-\alpha(m-n-1)}{1+\beta n}\right)\sigma_{01}(\varepsilon + E_{01} - E_{nm}) \quad (2)$$

In this formula, $E_{01} = E_1 - E_0$ and $E_{nm} = E_m - E_n$ are the threshold energies for excitation from level $\upsilon = 0$ to $\upsilon = 1$ and for excitation from level $\upsilon = n$ to $\upsilon = m$, respectively. Hence, the cross sections, $\sigma_{nm}(\varepsilon)$, are calculated from the cross section $\sigma_{01}(\varepsilon)$ for excitation from the ground state to the first vibrational level by shifting this cross section $\sigma_{01}(\varepsilon)$ over an energy of $E_{01} - E_{nm}$ and by adapting the value with an exponential factor. The parameters α and β are specific for each plasma species. For CO_2, α is taken as 0.5 and β is 0,[30] whereas for N_2, α is taken as 0.7 and β is 0.05.[1] For CO and O_2, we do not need to use this formula, as the cross sections are described in the literature; more information can be found in Kozák and Bogaerts.[30]

2.2.2.2. VT Relaxation Processes of the Vibrational Levels. In vibrational−translational (VT) relaxation, the internal vibrational energy is transferred into translational energy upon collision of a vibrationally excited species with another species. In the case of CO_2 splitting, this process should be avoided because it lowers the population of the higher vibrational levels, which otherwise give rise to dissociation (see below). As the rate coefficient of VT relaxation is determined by the gas temperature, this process can be reduced by using a lower gas temperature in the plasma.[1]

We assume in our model that at maximum one quantum of vibrational energy is transferred between the collision partners in VT relaxation processes because so-called multiquantum processes typically have a rate that is 2 orders of magnitude lower.[30] The rate coefficients for VT relaxation of the CO_2 vibrational levels upon collision with other CO_2 molecules, or with CO or O_2 molecules, are adopted from Kozák and Bogaerts.[30] As described in ref 30, the rate coefficient for collisions with CO and O_2 molecules was taken to be equal to the rate coefficient for collisions with CO_2 but multiplied by a factor of 0.3 (for CO) or 0.4 (for O_2).[43] The same approach is used here for collisions with N_2 molecules, i.e., the rate coefficient is taken to be equal to the rate coefficient for collisions with CO_2, but multiplied by a factor of 0.3.[43] The rate coefficients for VT relaxation of the CO vibrational levels with CO, CO_2, and O_2 are also adopted from ref 30. For collisions with N_2, the rate coefficients are taken to be the same as for collisions with O_2, based on ref 43.

For the higher vibrational levels of CO_2 and CO, the rate coefficients are calculated with a scaling law, based on the Schwartz−Slawsky−Herzfeld (SSH) theory for collisions between two anharmonic oscillators,[44] as described in detail in ref 30. The rate coefficients for VT relaxation of the N_2 and O_2 vibrational levels with either CO_2, CO, O_2, or N_2 are calculated with the forced harmonic oscillator (FHO) model,[45,46] which compares well with exact quantum methods.[47]

More details about the VT relaxation processes and the corresponding rate coefficients can be found in ref 30, as well as in Table A1 of the Supporting Information, for the VT reactions that were incorporated in this model for the CO_2/N_2 mixture.

2.2.2.3. VV Relaxation Processes of the Vibrational Levels. In vibrational−vibrational (VV) relaxation, the internal vibrational energy of one species is transferred to another species upon collision. This process is very important in CO_2 splitting, as it populates the higher vibrational levels out of the lower levels, which are populated by electron impact excitation (see above).[1]

Like for VT relaxation, we assume again that at maximum one quantum of vibrational energy is transferred between the collision partners in VV relaxation.[30] The rate coefficients for the lower vibrational levels are again adopted from the literature.[30,44] For the higher vibrational levels, we again use the SSH theory to calculate the rate coefficients of VV relaxation for collisions between two CO_2 vibrational levels and

DOI: 10.1021/acs.jpcc.5b01466
J. Phys. Chem. C 2015, 119, 12815−12828

between CO_2 and CO levels, assuming that only short-range interactions are important. For collisions of CO_2−N_2 and CO−CO, we must take into account both long-range and short-range interactions; therefore, we use a combination of the SSH theory and Sharma−Brau (SB) theory[48] for calculating the rate coefficients of VV relaxation of the higher vibrational levels. The rate coefficients for VV relaxation between two O_2 levels and two N_2 levels are again calculated with the FHO model.[45,46] The other combinations of VV relaxation (i.e., N_2−CO, N_2−O_2, CO−O_2, and CO_2−O_2) are not considered in our model, as they are assumed to be less important. Indeed, for the first three types of reactions, we have calculated the VV rate constants using the FHO model to find out that they are more than 2 orders of magnitude lower than the rate constants of the above-mentioned reactions. Moreover, the reactants CO and O_2 typically have densities that are lower than that of the inlet gases CO_2 and N_2. Their density is comparable to the densities of CO_2 and N_2 only later in the simulations and for high-power densities.

Again, the details about the VV relaxation processes and the corresponding rate coefficients can be found in ref 30, as well as in Table A2 of the Supporting Information, for the extra VV reactions included in this model for the CO_2/N_2 mixture.

2.2.2.4. Chemical Reactions of the Vibrational Levels. Finally, also chemical reactions of the vibrational levels need to be taken into account. Their rate coefficients are typically calculated from the corresponding rate coefficients of the collisions from the ground-state atoms by multiplying with an exponential factor according to the Fridman−Macheret α-model.[1] This yields the following formula:

$$k_R(E_v, T) = A^* \exp\left(\frac{-E_A - \alpha E_v}{T}\right) \quad (3)$$

where A is the pre-exponential factor, E_A the activation energy, E_v the vibrational energy, and T the gas temperature; α represents the efficiency of the vibrational level to lower the activation energy, adopted from refs 1 and 30. For reactions where no α could be found, we make the same assumptions as described by Fridman,[1] i.e.

- When no bond breaking occurs, α is taken equal to a very low value (0.03).
- When bond breaking occurs in the vibrationally excited species, α is taken as 0.9.
- When in addition to the bond breaking also an atom is transferred, α is taken as 1.0.

2.3. Application of the 0D Model to a MW Reactor. As mentioned in the beginning of this section, a 0D model calculates only the species densities as a function of time, and it neglects spatial variations. However, the time evolution can be translated into a spatial evolution (i.e., as a function of position in the MW reactor) by means of the gas flow rate. Indeed, the MW reactor can be considered to be a tubular reactor in which the densities vary only in the axial direction but remain constant in the radial direction. The plasma reactor is thus treated as a plug flow reactor. In this way, axial variations in power density can be implemented in the model without adding to the computational cost. The electron density in the radial direction may change by a factor of 2 or 3 in the bulk plasma.[49−52] These fluctuations in electron density, however, do not affect the plasma chemistry, as is shown in the Supporting Information. The CO_2/N_2 gas mixture is inserted at the inlet of the tubular reactor, and on their way throughout the reactor, the gases will gradually be converted into the reaction products, which leave the reactor at the other side. In other words, the time has the meaning of residence time of the species in the reactor.

The electric power in the MW plasma is applied to the electrons by setting a certain value for the reduced electric field, assuming the electric field frequency is equal to 2.45 GHz. The reduced electric field is calculated at each time step to obtain the desired axial distribution of the power density and the desired total power deposition. The maximum of the power density is applied in the center of the reactor (where the waveguide crosses the reactor tube in reality). Furthermore, we assume that the power density decreases linearly toward both ends of the discharge tube in accordance with theoretical calculations.[53] This is illustrated in Figure 1 for the three different power density values investigated, i.e., 30, 50, and 80 W/cm^3.

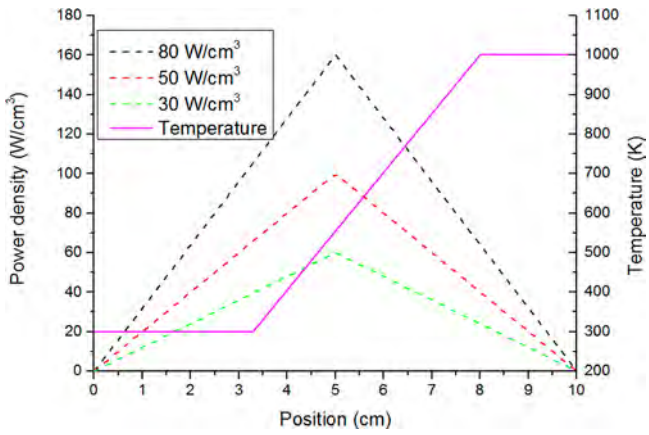

Figure 1. Power density profile (dashed curves; left axis) and temperature profile (solid curve; right axis) used in the simulations.

The operating conditions assumed in the model, i.e., power density, gas flow rate, pressure, and temperature, are exactly the same as those used in the experiments (see section 3). The gas flow rate is 5 slm for a MW reactor length of 10 cm. The pressure is taken as 2660 Pa,[6,7] and the gas temperature at the inlet is set at 300 K. Because the gas absorbs the most power in the center of the reactor, we assume that the gas temperature rises linearly between 3.3 and 8 cm, from 300 K to 1000 K (see solid curve in Figure 1), based on our earlier findings.[7,31]

3. EXPERIMENTAL SETUP

The surfaguide-type microwave discharge was generated at a frequency of 915 MHz in a double-walled quartz tube with 14 mm inner diameter and about 20 cm length, cooled during the measurements by 10 °C silicon oil flow (see Figure 2). The gas mixture injected from the top of the system was regulated by electronic mass flow controllers. The whole system was surrounded by a grounded aluminum grid to prevent any leak of microwave radiation into the surrounding space. At the bottom of the quartz tube, an additional diaphragm was installed to maintain the pressure difference between the discharge and the postdischarge regions.

The concentrations of CO_2, CO, and N_2 were analyzed by a gas chromatograph (Bruker) equipped with a carbon molecular sieve column and a Molecular sieve 5A column in series and connected to a thermal conductivity detector with argon used

DOI: 10.1021/acs.jpcc.5b01466
J. Phys. Chem. C 2015, 119, 12815−12828

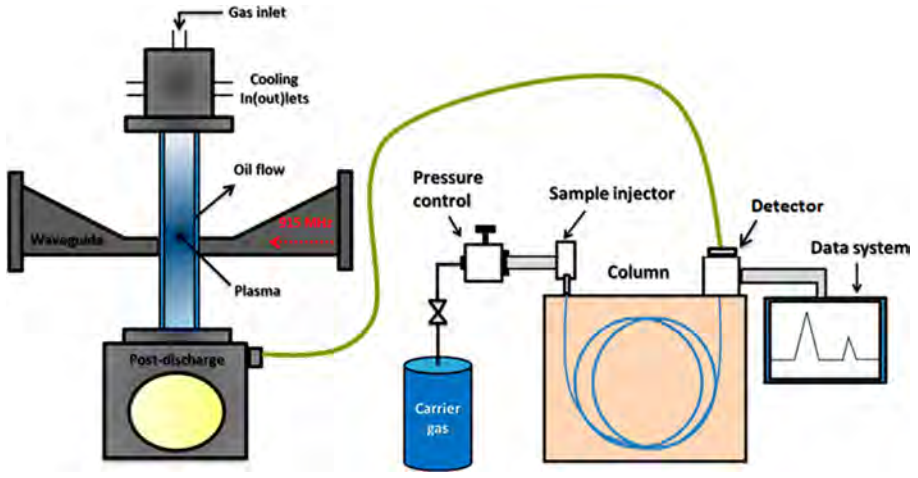

Figure 2. Schematic representation of the microwave generator and the gas chromatograph.

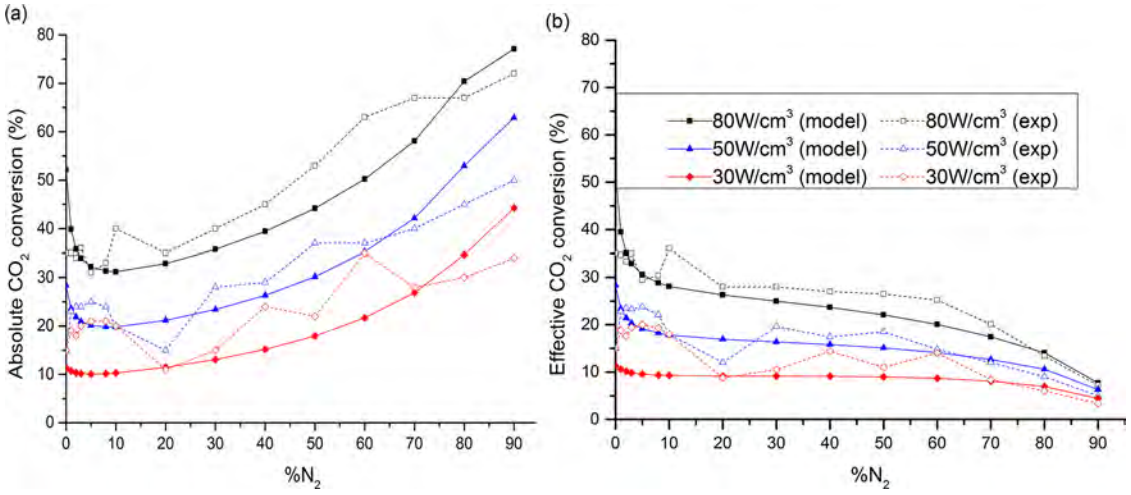

Figure 3. Calculated (solid lines) and measured (dashed lines) absolute (a) and effective (b) CO_2 conversion as a function of N_2 fraction in the gas mixture for three different power densities, a pressure of 2660 Pa, and a residence time of 9.13 ms.

as a carrier gas (see Figure 2). As the discharge worked in reduced pressure regime, a sampling system was used between the post discharge and the gas chromatograph. The low-pressure sample is diluted with neutral gas prior to its injection in the chromatograph.

4. RESULTS AND DISCUSSION

4.1. CO_2 and N_2 Conversion. The (absolute) conversion (χ_A) of a compound (CO_2 or N_2) is calculated from the number densities before and after the simulation:

$$\chi_A = 1 - \frac{n_A}{n_{A0}} \tag{4}$$

On the other hand, the effective conversion of a compound ($\chi_{A,eff}$) denotes how much is effectively converted and takes into account the fraction of the compound in the gas mixture, e.g., when only 10% CO_2 is present in the gas mixture, the absolute conversion needs to be multiplied by a factor 0.1. In this section, we will show both the absolute and effective conversion for both CO_2 and N_2.

Figure 3 illustrates the calculated and measured absolute and effective CO_2 conversions as a function of N_2 fraction in the gas mixture for the three different values of power density investigated, i.e., 30, 50, and 80 W/cm^3. In general, agreements within 23% with the measured values are obtained. The largest deviations occur at N_2 fractions below 10%, with discrepancies reaching 70%. However, the overall evolution of the calculated CO_2 conversion with rising N_2 fraction follows the experimental results. This indicates that the plasma chemistry and vibrational kinetics occurring in the microwave plasma are quite realistically described in our model.

It is clear that the absolute conversion (Figure 3a) increases with N_2 fraction, both in the model and the experiments, indicating that N_2 has a beneficial effect on the conversion, as will be discussed in sections 4.3 and 4.4. However, at the higher power densities, a slight drop in the calculated CO_2 conversion is seen between 0% and 10% N_2, which can be explained by the model based on the relative contributions of the CO_2 destruction mechanisms, as will be discussed in section 4.3. However, this slight drop is not so visible in the experimental data, so it might be overestimated in the model.

The effective CO_2 conversion (Figure 3b) generally drops upon increasing N_2 fraction, which is as expected because there is less CO_2 initially present in the gas mixture. However, this drop is not very pronounced, especially not between 10 and 60% N_2, because of the rising absolute conversion, as observed in Figure 3a. In general, the CO_2 conversion is very high (i.e., 10−80% absolute conversion and 5−53% effective conversion,

DOI: 10.1021/acs.jpcc.5b01466
J. Phys. Chem. C 2015, 119, 12815−12828

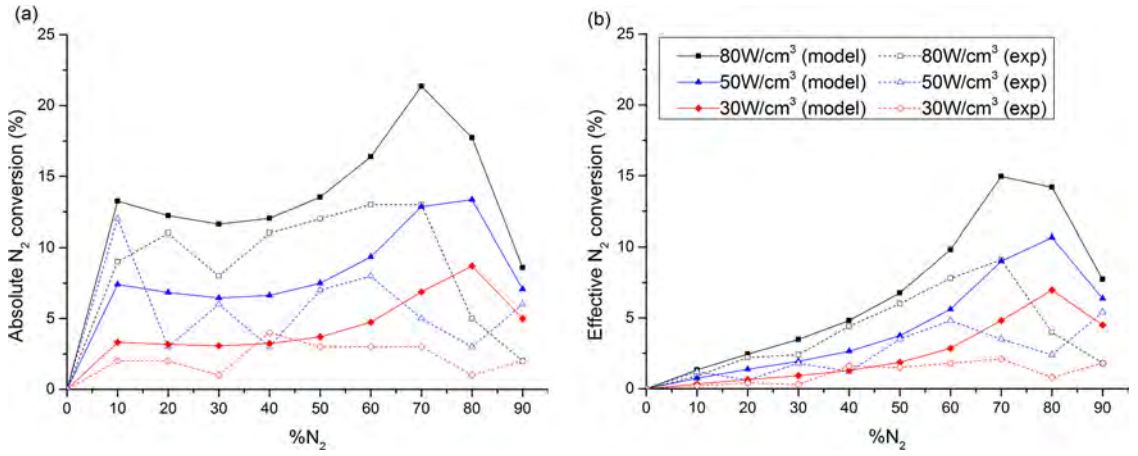

Figure 4. Calculated (solid lines) and measured (dashed lines) absolute (a) and effective (b) N_2 conversion as a function of N_2 fraction in the gas mixture for the same conditions as in Figure 3.

depending on power and N_2 fraction), and it increases clearly with rising power density, as expected.

The calculated and measured absolute and effective N_2 conversions are plotted as a function of N_2 fraction in the gas mixture in Figure 4 for the three different values of power density. Agreements between calculated and measured results are generally within 33%, and thus somewhat worse than for the CO_2 conversion. The largest deviations (i.e., up to 130%) occur at 80% N_2 where the model systematically predicts values higher than the experiment values. This indicates that the model might still need further improvement, although the experiments are also subject to uncertainties. However, the focus of this paper is more on obtaining a better insight into how N_2 interacts with CO_2, especially its effect on the vibrational kinetics, and less on the N_2 conversion itself.

The N_2 conversion increases again clearly with power density, as expected. The absolute N_2 conversion is rather constant for all power values, up to 50% N_2 fraction, and then it rises to 70−80% N_2 fraction, followed by a significant drop toward 90% N_2 fraction in the gas mixture. In the model, this trend is explained by the fact that the most important formation processes for N_2 are reactions between reactive N-compounds, which originate from the destruction of N_2 (see section 4.3).

The effective N_2 conversion generally rises with N_2 fraction, which is logical as there is more N_2 initially present in the gas mixture, but the same drop is observed above 70−80% N_2 fraction, which follows of course the behavior of the absolute conversion. The highest effective N_2 conversion is around 15% (calculated) and 9% (measured) at the highest power density and a N_2 fraction of 70%. This indicates that under these conditions the formation of reactive N-compounds will be at a maximum, including also NO_x species.

Indeed, our model predicts that above 70% N_2 addition, some reactive N-compounds are formed. The most abundant is NO, with a relative percentage (among the formed products) of 40−50%, followed by C_2N_2 and CN, with relative percentages of 15−20% and 5−10%, respectively. Other NO_x compounds, like NO_2, NO_3, N_2O and N_2O_5, were found to be negligible, as predicted by the model.

4.2. Energy Efficiency. The energy efficiency will be presented only for the CO_2 conversion because this is the process of major importance in this study. It is calculated from the effective CO_2 conversion as

$$\eta = \chi_{A,\mathrm{eff}} \frac{\Delta H}{\mathrm{SEI}} \tag{5}$$

where ΔH is the theoretical reaction enthalpy for CO_2 splitting ($CO_2 \rightarrow CO + 1/2\ O_2$), i.e., 2.9 eV/molec, and SEI is the specific energy input for the process. The latter is calculated in the model by integrating the power deposition (P_d, in W/cm^3) over the residence time (t_r):

$$\mathrm{SEI}\left(\frac{\mathrm{J}}{\mathrm{cm}^3}\right) = \int_0^{t_r} P_d\, dt = \int_0^{t_r} e{*}E/N{*}\nu_d{*}n_e{*}\mathrm{N}\, dt \tag{6}$$

where e is 1.6×10^{-19} J/(e)V), E/N the reduced electric field (in Td or 10^{-17} V cm^2), ν_d the drift velocity of the electrons (cm s^{-1}), n_e the electron number density (cm^{-3}), and N the number density of the neutral species (cm^{-3}). The SEI (in eV/molec) is calculated as follows:

$$\mathrm{SEI}\left(\frac{\mathrm{eV}}{\mathrm{molecule}}\right) = \frac{\mathrm{SEI}\left(\frac{\mathrm{J}}{\mathrm{cm}^3}\right)}{e{*}t_r{*}Q_n} \tag{7}$$

where Q_n is the gas density flow rate (no. molec/(cm^3 s)), which is calculated as

$$Q_n = \frac{p}{t_r k_B T_{gas} 10^6} \tag{8}$$

where p is the gas pressure (Pa), k_B the Boltzmann constant, and T_{gas} the neutral gas temperature (K). The factor 10^6 is used to transfer Q_n from no. molec/(m^3 s) to no. molec/(cm^3 s). The three power densities investigated, i.e., 30, 50, and 80 W/cm^3, correspond to SEI values of 2.66, 4.44, and 7.1 eV/molec, respectively.

Figure 5 illustrates the calculated and measured energy efficiencies for CO_2 conversion for the three different power densities and the entire range of CO_2/N_2 gas mixing ratios. Agreements within 23% are obtained between model and experiments. The largest deviations (i.e., 70%) occur at low N_2 fractions, similar to the results of the effective CO_2 conversion, which is logical, considering eq 5.

The energy efficiency is in the order of 8−15%, except at the highest N_2 fractions, where it drops to 3%. Furthermore, the calculated values drop slightly from 0 to 10% N_2 fraction at the lowest power density (i.e., by ∼2%), and this drop is more significant for 50 and 80 W/cm^3 (i.e., around 7% and 10%, respectively). However, this trend was not observed in the

DOI: 10.1021/acs.jpcc.5b01466
J. Phys. Chem. C 2015, 119, 12815−12828

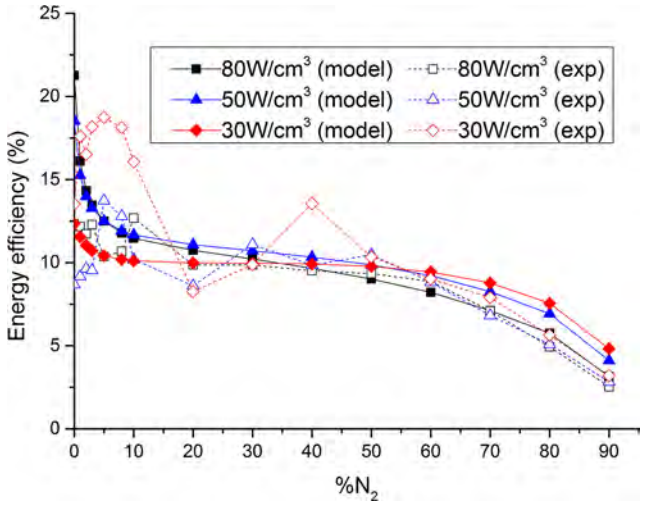

Figure 5. Calculated (solid lines) and measured (dashed lines) energy efficiencies for CO_2 conversion as a function of N_2 fraction in the gas mixture, for the same conditions as in Figure 3.

experiments, mainly because of a rather high measurement error in this case. Between 10% and 60% N_2 fraction, the energy efficiency drops slightly, but at higher N_2 fractions, the drop is again a bit more pronounced. These trends can again be explained based on the relative contributions of the CO_2 destruction processes, as discussed in section 4.3. The calculated energy efficiency at low N_2 fractions is highest for the higher power densities, whereas the opposite trend is seen for the high N_2 fractions, although the differences are small. This behavior will also be explained in sections 4.3 and 4.4.

When comparing these energy efficiencies with values from the literature, albeit for pure CO_2 MW plasmas, we can conclude that the maximum obtained calculated energy efficiency (i.e., 21% at 80 W/cm^3 or an SEI of 7.1 eV/molec) is similar to the value predicted by Kozák and Bogaerts[30] (i.e., 23%; the small difference is attributed to the use of a different 0D code, with other approximations[30]). Several years ago, Fridman and colleagues[1,13,14] reported much higher values of 90% for a MW reactor, but the latter was operating under supersonic flow conditions. However, at normal flow conditions, values similar to those obtained here were also reported.[1,7] Indeed, for a pressure of 50 Torr (or 6664 Pa), a value of 20% was obtained.[1] Furthermore, earlier experiments by Silva et al.[7] yielded energy efficiencies of 12% for a pulsed MW plasma at a pressure in the range of 133−1333 Pa and a SEI in the range of 25−40 eV/molecule.

4.3. Destruction and Formation Processes of CO_2 and N_2. From the comparison between calculated and experimental data, we can conclude that the model is in general able to qualitatively and even quantitatively describe the most important chemical reactions in the CO_2/N_2 plasma and can thus be used for explaining the underlying mechanisms responsible for the experimental trends in CO_2 and N_2 conversion and in the energy efficiency. This will be elaborated here and in the following sections.

To explain the trends in the CO_2 and N_2 conversion, we plot in Figure 6 the relative contributions of the most important destruction processes of CO_2, as a function of N_2 fraction, for 30 W/cm^3 and 80 W/cm^3. The results of 50 W/cm^3 s are intermediate, so they are not explicitly presented.

At the two highest power densities, the destruction of CO_2 is mainly attributed to the dissociation of vibrationally excited CO_2 by collision with any molecule in the plasma (denoted as M). At 30 W/cm^3, this process is also important for N_2 fractions above 30%. At lower N_2 fractions, electron impact dissociation from ground-state CO_2, and especially from vibrationally excited CO_2, are more important, with a contribution of 25% and 42%, respectively. At 50 and 80 W/cm^3 and N_2 fractions below 20%, electron impact dissociation from vibrationally excited CO_2 is also very important for the CO_2 destruction, with a contribution of about 33% around 10% N_2, at both 50 and 80 W/cm^3. At higher N_2 fractions, these processes gradually become less important upon increasing N_2 fraction.

Because electron impact dissociation from the CO_2 ground state requires considerably more energy than the dissociation energy of CO_2, this explains the lower energy efficiency at 30 W/cm^3 and low N_2 fractions, as shown in Figure 5.

Finally, the reaction between vibrationally excited CO_2 and an O atom is also significant, with a contribution of 10−28% and slightly increasing for higher N_2 fractions. The difference between this process and the dissociation reaction with any molecule M is that in the first process the formed O atoms

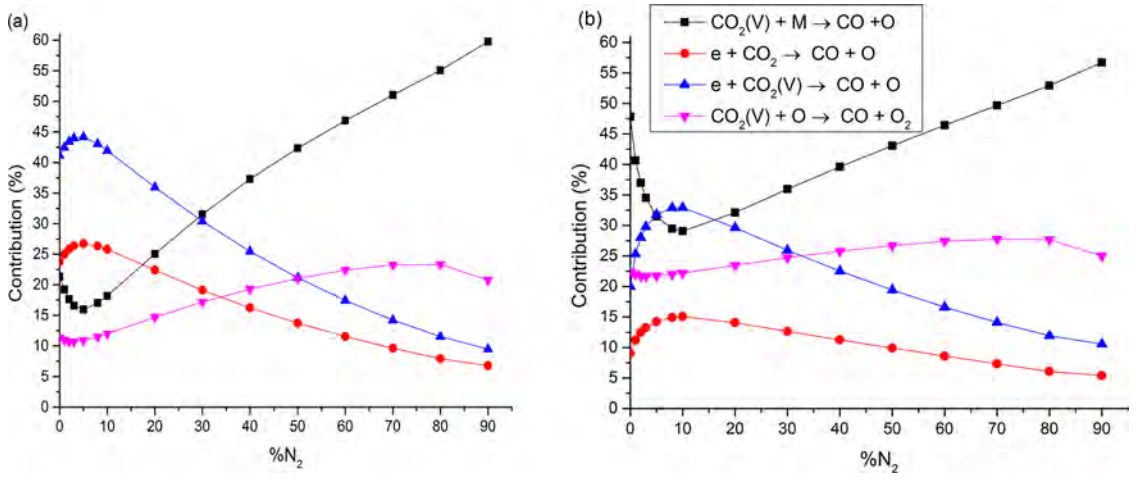

Figure 6. Relative contributions of the most important destruction processes of CO_2, as a function of N_2 fraction in the gas mixture, for the same conditions as in Figure 3 and for the power density of 30 W/cm^3 (a) and 80 W/cm^3 (b).

DOI: 10.1021/acs.jpcc.5b01466
J. Phys. Chem. C 2015, 119, 12815−12828

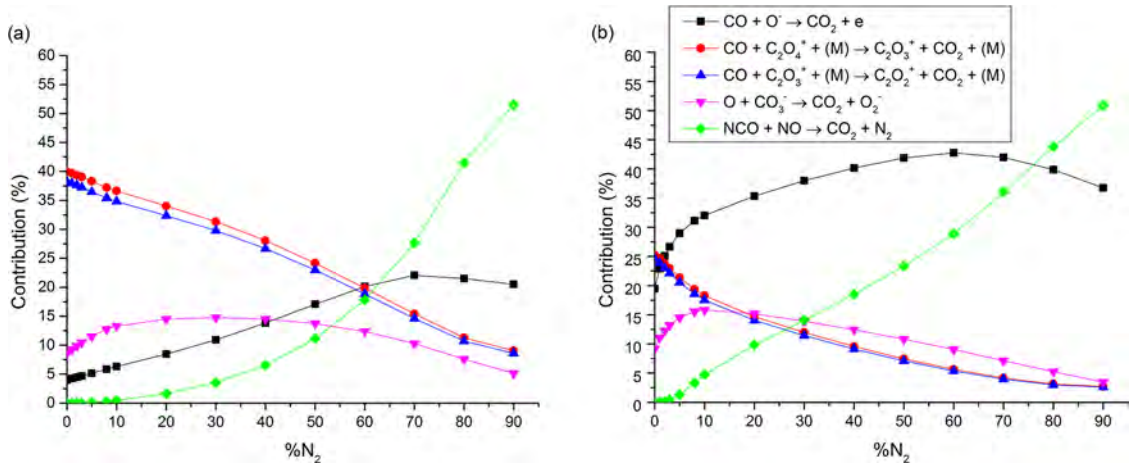

Figure 7. Relative contributions of the most important formation processes of CO_2 as a function of N_2 fraction in the gas mixture for the same conditions as in Figure 3 and for the power density of 30 W/cm^3 (a) and 80 W/cm^3 (b).

recombine with the reactant O atoms, forming O_2, whereas in the latter process no such recombination of O atoms occurs. Note that this first reaction is essential for the total CO_2 conversion into CO and O_2, which is in fact the combination of two subsequent steps:

(1) $CO_2 \rightarrow CO + O$ (upon collision of an electron, followed by VV relaxation (i.e., so-called ladder climbing), or upon collision with any neutral molecule)
(2) $CO_2 + O \rightarrow CO + O_2$

It is the combination of these two steps that is considered for the calculation of the energy efficiency. Indeed, the reaction enthalpy needed for the first reaction is 5.5 eV/molec, while for the second reaction only 0.3 eV/molec is needed.[1] In total, this gives a reaction enthalpy of 2.9 eV/molecule per one CO_2 molecule, which is the value used for calculating the energy efficiency (see section 4.2).

For the three power densities investigated, the contribution of the neutral reactions with vibrationally excited CO_2 (i.e., either by collision with M or O atoms) is slightly lower at 10% N_2 fraction than for the pure CO_2 plasma, but it increases again for higher N_2 fractions. The reason for this drop between 0 and 10% N_2 fraction will be clarified based on the vibrational distribution functions, shown in section 4.4. This drop also explains the calculated drop in both the absolute and effective CO_2 conversion from 0% to 10% N_2, as illustrated in Figure 3. At 30 W/cm^3, this drop in effective and absolute CO_2 conversion was barely visible (~1%), because of the lower contribution of this reaction (see Figure 6a).

Neutral reactions with vibrationally excited species are more energy-efficient than electron impact dissociation.[1] Therefore, a drop in the contribution of the reaction ($CO_2(V) + M \rightarrow CO + O$) also explains the drop in energy efficiency, predicted by the model, between 0% and 10% N_2 at the higher power densities, where this process is dominant, as was illustrated in Figure 5.

The fact that the effective CO_2 conversion and energy efficiency remain constant between 10% and 60% at 30 W/cm^3 and drop to some extent in the same interval at 50 and 80 W/cm^3, as shown in Figures 3 and 5, can be explained based on the fact that the sum of the relative contributions of the three reactions with vibrationally excited CO_2 (which are most beneficial for the energy efficiency) rises faster or slower with increasing N_2 fraction than the drop in the contribution of the less energy-efficient electron impact dissociation from the ground state. Indeed, at 50 and 80 W/cm^3, there is a clear drop in effective CO_2 conversion and energy efficiency because the relative contribution of electron impact dissociation drops faster with rising N_2 fraction than the rise in relative contributions of the three reactions with vibrationally excited CO_2. This results in a higher contribution of very energy-inefficient processes, like the reactions between ions and ionization of the N_2 fraction, and hence in a more pronounced drop of the energy efficiency for CO_2 splitting. This effect is the strongest at 80 W/cm^3, as can be seen in Figure 5. On the other hand, at 30 W/cm^3, the contribution of the vibrational reactions increases to the same extent as the drop in electron impact dissociation from the ground state; therefore, the effective CO_2 conversion and energy efficiency remain more or less constant upon rising N_2 fraction, as was indeed illustrated in Figures 3 and 5.

Above 60% N_2, the contribution of the vibrational reactions will rise more slowly than the drop in the contribution of electron impact dissociation from the ground state for all three power densities; therefore, the energy efficiency will again drop faster. As this effect is the strongest at 80 W/cm^3, the energy efficiency will drop faster in this case, upon increasing N_2 fraction, as is clear from Figure 5.

Figure 7 illustrates the relative contributions of the most important formation processes of CO_2, as a function of N_2 fraction, again for 30 and 80 W/cm^3. At 80 W/cm^3, the reaction between (ground-state or vibrational) CO and O^- ions, with the formation of CO_2 and an electron, is the most important formation process in almost the entire range of N_2 fractions (see Figure 7b). This is also the case for 50 W/cm^3, at least between 20% and 70% N_2 (not shown). For the lower N_2 fractions (i.e., < 20% N_2 at 50 W/cm^3 and <2% N_2 at 80 W/cm^3), the reactions of $C_2O_4^+$ or $C_2O_3^+$ ions with CO are more important. At 30 W/cm^3, these two reactions are by far the most important below 60% N_2 (see Figure 7a). Finally, the reaction between NCO and NO, with the formation of CO_2 and N_2, is the dominant formation process at very high N_2 fractions when there are enough reactive N-compounds present. However, it should be mentioned that the relative contribution of the formation processes should not be overestimated, as the total formation rate of CO_2 is 2 orders of magnitude lower than the total destruction rate.

DOI: 10.1021/acs.jpcc.5b01466
J. Phys. Chem. C 2015, 119, 12815−12828

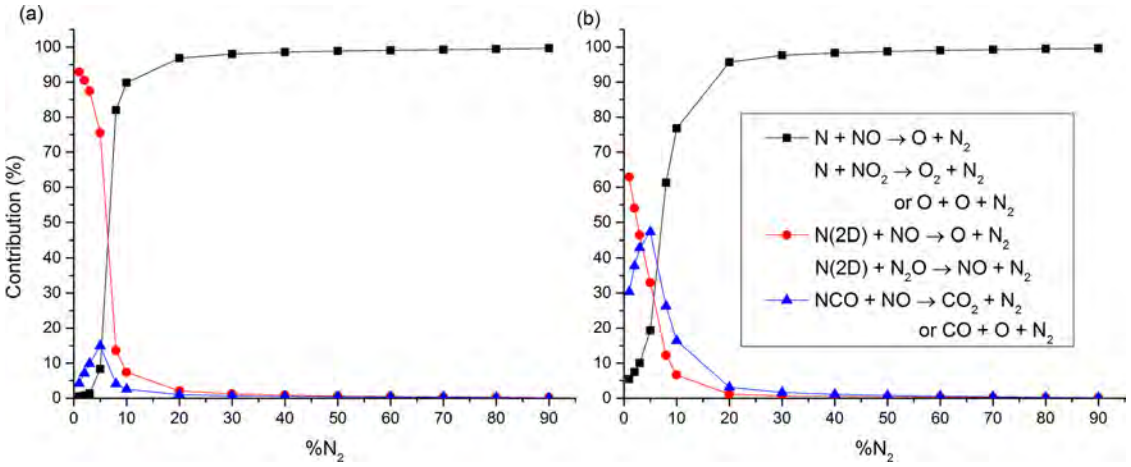

Figure 8. Relative contributions of the most important formation processes of N_2 as a function of N_2 fraction in the gas mixture for the same conditions as in Figure 3 and for the power density of 30 W/cm^3 (a) and 80 W/cm^3 (b).

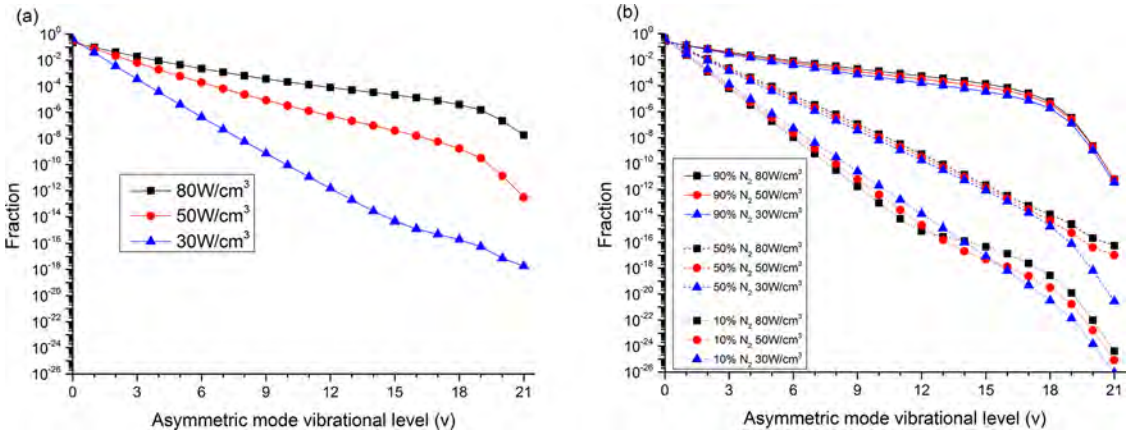

Figure 9. Vibrational distribution functions (VDFs) of the asymmetric mode vibrational levels of CO_2, obtained at the end of the simulations (i.e., a position of 10 cm), for three different power densities and N_2 fractions of 0% (a) and 10%, 50%, and 90% (b).

N_2 is almost exclusively destroyed by the reaction between vibrationally excited N_2 molecules and O atoms, yielding the formation of N and NO. The relative contribution of this process is above 95% for all N_2 fractions and power densities investigated. The contributions of the three most important formation processes are depicted in Figure 8 for 30 and 80 W/cm^3. The reaction of N atoms with either NO or NO_2, yielding O atoms or O_2 molecules, besides the N_2 molecules, is the dominant formation process for all power densities investigated and for N_2 fractions above 10%. At lower fractions, N_2 is mainly formed by the reaction of N(2D) with NO or N_2O, forming O atoms or NO radicals, besides N_2. At 80 W/cm^3, the reaction between NCO and NO, forming N_2 and either CO_2 or CO and O atoms, also plays a role.

Note that in contrast to CO_2, the total formation rate of N_2 is not so much lower than the total destruction rate, i.e., it is at maximum a factor 3 lower at 20% N_2. The difference becomes even smaller with rising N_2 fraction, i.e., at the highest N_2 fraction investigated, the total formation and destruction rates are almost equal to each other. The net destruction rate (i.e., destruction rate minus formation rate) increases with rising N_2 fraction, up to 70% N_2 at the power density of 80 W/cm^3 and up to 80% N_2 at the lower power densities, but it decreases for still higher N_2 fractions because of the higher densities of reactive N-compounds (N, NO, NO_2) responsible for forming N_2 again. This explains the calculated drop in N_2 conversion above 70% N_2 (for 80 W/cm^3) and above 80% N_2 (for the lower power densities) shown in Figure 4.

4.4. Vibrational Analysis of CO_2. It is clear from the previous section that the vibrational levels of CO_2 play a crucial role in the CO_2 splitting process. Therefore, it is important to investigate the vibrational distribution function (VDF) of CO_2 at the various power densities and to elucidate which processes are responsible for populating these vibrational levels and whether N_2 will play a role in determining the VDF of CO_2. As the asymmetric mode vibrational levels are most important for the dissociation of CO_2, we will focus only on the VDF of these 21 asymmetric mode levels. In Figure 9, the VDFs, obtained at a position of 10 cm, are depicted for the three different power densities at N_2 fractions of 0% (Figure 9a) and 10%, 50%, and 90% (Figure 9b).

At 0% N_2, the populations of the higher vibrational levels are much lower at 30 W/cm^3 than at 50 and 80 W/cm^3. The total percentage of vibrationally excited CO_2 is 60% at 30 W/cm^3, while it is 72% and 77% at 50 and 80 W/cm^3, respectively. This explains why vibrationally excited CO_2 is so important for CO_2 splitting in a MW plasma, especially at the higher power densities (cf. Figure 6).

At 10% N_2 (Figure 9b), the VDFs are very close to each other for the three power densities investigated, with only a

DOI: 10.1021/acs.jpcc.5b01466
J. Phys. Chem. C 2015, 119, 12815−12828

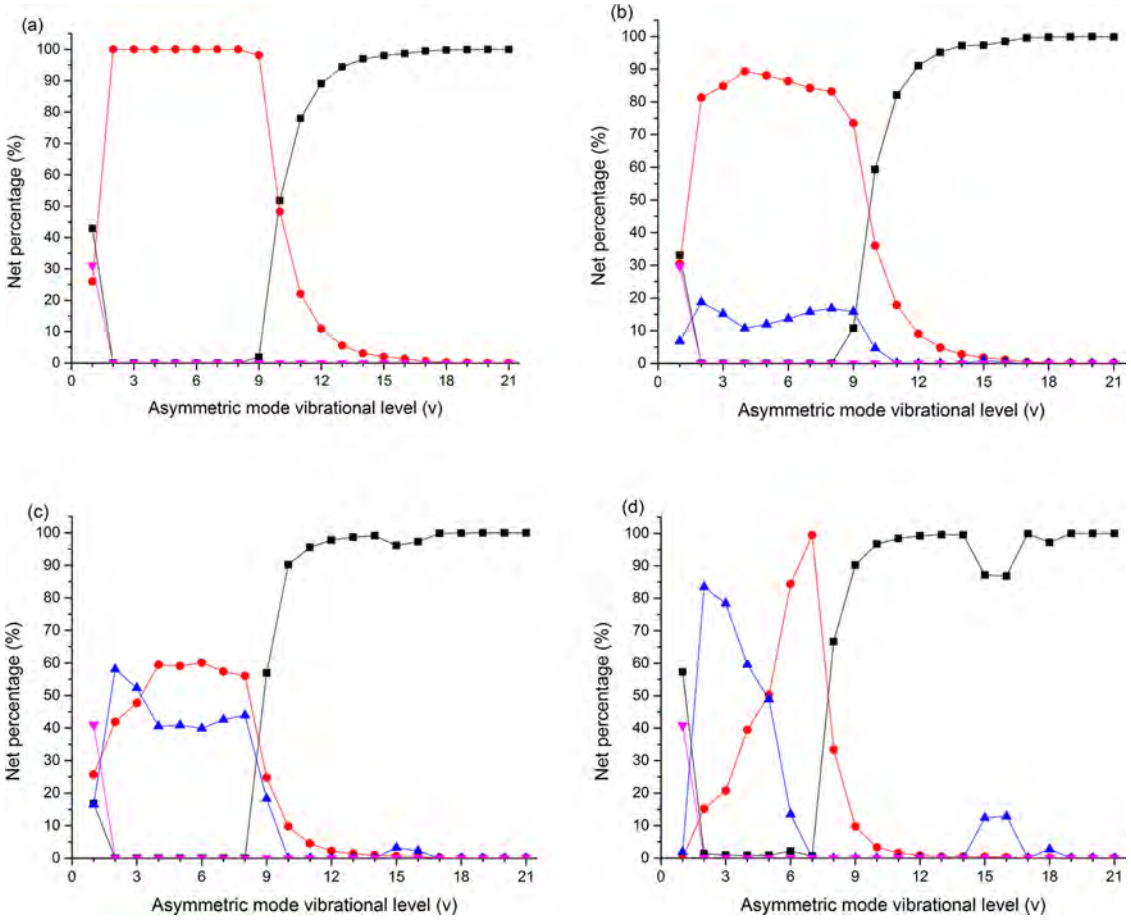

Figure 10. Relative contributions of the various processes responsible for the population of the asymmetric mode vibrational levels of CO_2 at 80 W/cm^3 and N_2 fractions of 0% (a), 10% (b), 50% (c), and 90% (d).

slightly higher population of the highest vibrational levels upon increasing power density. The fractions of the vibrational levels are 56%, 55%, and 55% at the power densities of 30, 50, and 80 W/cm^3, respectively. This is lower than at 0% N_2, which explains the drop in the contribution of the reaction between CO_2(V) and neutral molecules M (i.e., $CO_2(V) + M \rightarrow CO + O + M$), compared to the pure CO_2 case, as was illustrated in Figure 6.

At 50% N_2, the difference between the VDFs obtained at the different power densities is even lower than at 10% N_2, and at 90% N_2, they are almost equal to each other, as appears also from Figure 9b. The fractions of vibrationally excited CO_2 for the three different power densities are calculated to be 63%, 63%, and 64% at 50% N_2, and 73%, 73%, and 74% at 90% N_2. It is curious that in the case of 90% N_2 at 80 W/cm^3 the percentage of vibrationally excited CO_2 is lower than at the same power density at 0% N_2, and yet the contribution of neutral reactions with vibrationally excited CO_2 is higher. This is because at 0% N_2 a lower fraction of the vibrationally excited CO_2 is found in the higher levels, when compared to 90% N_2. This again stresses the importance of the high vibrationally excited CO_2 levels. In the other cases, more vibrationally excited CO_2 also means more highly vibrationally excited CO_2, and this gives rise to higher contributions of the destruction reactions involving vibrationally excited CO_2 (see Figure 6).

Because the VDFs of the different power densities are nearly equal to each other at 90% N_2, the importance of the vibrationally excited CO_2 levels is also equally important for the CO_2 splitting, as was clear from Figure 5. Therefore, at this higher N_2 fraction, the power density of 30 W/cm^3 will yield a higher energy efficiency (cf. Figure 5) because the vibrational levels are equally important, but the SEI is significantly lower.

To explain the VDFs at the various N_2 fractions and power densities, we make here an analysis of the processes responsible for the population of these vibrational levels. The relative contributions of the various mechanisms are plotted in Figure 10 as a function of the vibrational level at 80 W/cm^3 and various N_2 fractions. The results at the other power densities are almost equal and are therefore not shown.

At 0% N_2 (Figure 10a), the most important mechanisms for population of the higher levels, which are important for CO_2 splitting, are the VV relaxation processes with either CO_2 or CO vibrational levels. This was also reported by Kozák and Bogaerts.[30] For the lower levels (i.e., levels 2−9), electron impact vibrational excitation is the most important population mechanism, whereas the first vibrational level appears to be mainly populated by VT and VV relaxation from the higher levels.

At 10% N_2 (Figure 10b), we observe the same behavior: electron impact vibrational excitation is most important for the lower levels, and VV relaxation with CO_2 or CO vibrational levels is dominant for the higher levels. However, VV relaxation with N_2 now also contributes to some extent (∼15%), especially for the lower levels, so that the relative contribution of electron impact vibrational excitation drops slightly.

DOI: 10.1021/acs.jpcc.5b01466
J. Phys. Chem. C 2015, 119, 12815−12828

At 50% N_2, the contribution of VV relaxation with N_2 becomes comparable to electron impact vibrational excitation for the lower levels, and it is even slightly more important for the levels 2−4 at the highest power density of 80 W/cm^3 (which is effectively illustrated in Figure 10c). This is logical because a higher power density yields more vibrational excitation of N_2 (see section 4.5). The higher vibrational levels of CO_2, on the other hand, are still almost exclusively populated by VV relaxation with CO_2 and CO.

Finally, at 90% N_2, VV relaxation with N_2 becomes the dominant population mechanism for the lower CO_2 vibrational levels (level 2−4), at all power densities. For the higher levels, VV relaxation with CO_2 and CO is still most important, as is clear from Figure 10d. VT relaxation, although in general an important process, e.g., for the net vibrational energy losses and the associated heating of the gas, appears to be negligible for the net population of the vibrational levels at all power densities and N_2 fractions investigated because the VV rates are much faster than the VT rates.

Hence, we can conclude that for all power densities investigated, N_2 plays an important role in the population of the lower (asymmetric mode) vibrational levels of CO_2, especially at higher N_2 fractions. The reason is that at higher N_2 concentrations in the mixture, there is more electron impact vibrational excitation of N_2 compared to CO_2, and thus also a higher vibrational energy transfer rate between N_2 and CO_2. Subsequently, VV relaxation with CO and CO_2 will (partially) convert these lower levels into the higher vibrational levels, which are essential for energy-efficient CO_2 splitting.

4.5. Vibrational Analysis of N_2. As the vibrational levels of N_2 are quite important (~15−85% contribution) for populating the CO_2 vibrational levels and therefore for CO_2 splitting, we present in Figure 11 the VDFs of N_2, again obtained at a position of 10 cm, for 10%, 50%, and 90% N_2 in the gas mixture and at the power density of 80 W/cm^3. The results for the other power densities were virtually the same and are therefore not presented. This confirms that the role of vibrationally excited N_2 in populating the asymmetric mode vibrational levels for CO_2 will be almost the same for the different power densities (see previous section). As mentioned in section 2.2, only the lowest 14 levels of N_2 are considered, as the higher levels are negligible; this is indeed clear from Figure 11.

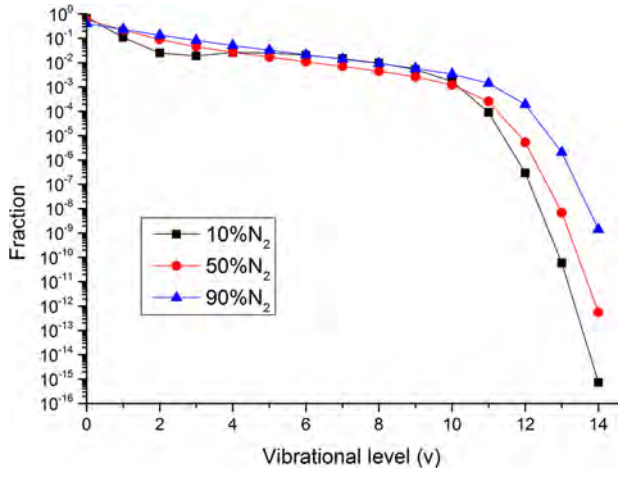

Figure 11. Vibrational distribution functions (VDFs) of N_2, obtained at the end of the simulations (i.e., a position of 10 cm), for N_2 fractions of 10%, 50%, and 90% and a power density of 80 W/cm^3.

We can deduce from Figure 11 that the VDFs look very similar to each other, except at the higher vibrational levels where the population becomes somewhat higher with increasing N_2 fraction. Nevertheless, the percentage of vibrationally excited N_2 rises with increasing N_2 fraction and is calculated to be 26%, 43%, and 59% for 10%, 50%, and 90% N_2, respectively. The reason for this rather large difference in the percentage of vibrationally excited N_2, although the VDFs seem similar, is because there is still a small yet significant rise in the population of the lower levels with increasing N_2 fraction. These levels are generally much more populated than the highest levels because of lower energy barriers, and a small change in their populations causes therefore a significant change in the total population in vibrationally excited N_2. The VDFs drop only slightly upon increasing level for the levels 1−11, but the populations of the higher levels are much lower. The reason is that for these higher levels, chemical reactions with vibrationally excited N_2 are important, which depopulate these levels, whereas the populations of the lower levels are mainly affected by electron impact excitation (see below), which does not give rise to such a drastic drop in the populations.

The relative contributions of the different processes responsible for the population of the various vibrational levels of N_2 are plotted in Figure 12, again for 80 W/cm^3 and for 10% and 90% N_2. The results at intermediate N_2 fractions are not shown because they are very much the same as for 90% N_2. Likewise, the results at the lower power densities are very similar to those for 80 W/cm^3 and are therefore not shown either. The most important population mechanism for the lower and intermediate vibrational levels (i.e., up to level 8−9) is electron impact vibrational excitation, with a contribution close to 100%, at all N_2 fractions and power densities investigated, while the higher levels are mainly populated by VV relaxation with either CO_2 or N_2. We want to stress the fact that the net contributions are plotted. The absolute contributions of the different populating and depopulating mechanisms for the intermediate and higher levels are dominated by VV relaxation with CO_2 and N_2. This means that when one of these levels is populated through VV relaxation with CO_2 and N_2 or vibrational excitation, depopulation immediately occurs by the same VV relaxation mechanisms or by chemical reactions. Therefore, averaged over the simulation time, the population due to VV relaxation is compensated by depopulation by the same mechanism because of the fast exchange of vibrational energy. This explains why vibrational excitation is even crucial as a net population mechanism for the intermediate levels of N_2.

We can deduce from Figure 12 that when the N_2 fraction in the gas mixture increases, VV relaxation with the CO_2 vibrational levels becomes more and more important for the N_2 levels 9−10. This is at first sight counterintuitive because we would expect that VV relaxation with the N_2 levels would become more important at higher N_2 fractions. The reason is that for higher N_2 fractions VV relaxation with N_2 vibrational levels becomes the most important depopulation mechanism for those levels, while VV relaxation with CO_2 and CO is relatively more important for depopulating the N_2 levels at lower N_2 fractions. This means that at higher N_2 fractions, VV relaxation with CO_2 and CO becomes more important as a net population mechanism. For the highest N_2 vibrational levels, on

DOI: 10.1021/acs.jpcc.5b01466
J. Phys. Chem. C 2015, 119, 12815−12828

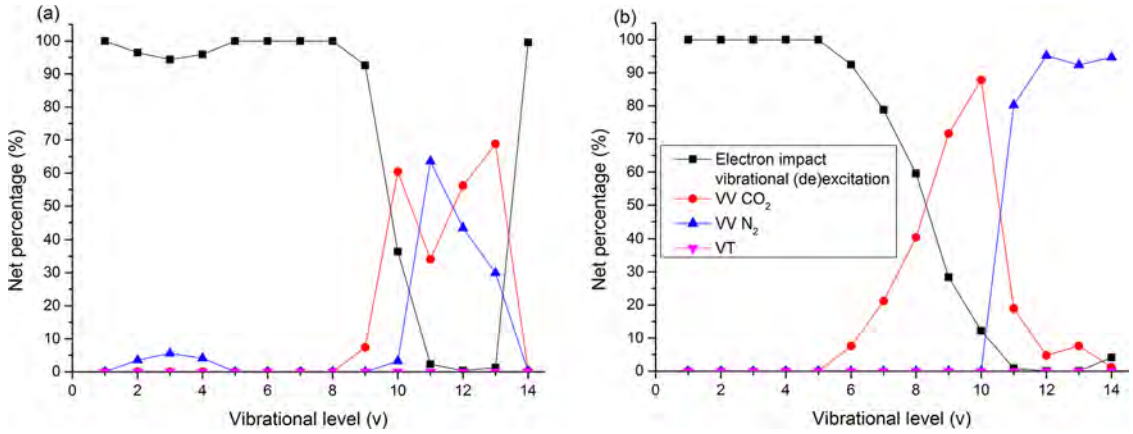

Figure 12. Relative contributions of the various processes responsible for the population of the N_2 vibrational levels, at 80 W/cm^3 and N_2 fractions of 10% (a) and 90% (b).

the other hand, VV relaxation with N_2 vibrational levels is the dominant net population mechanism at higher N_2 fractions (>50% N_2), as expected. However, as the populations of these levels are very low (see Figure 10), the absolute importance of these processes is almost negligible. Finally, as in the case for CO_2, VT relaxation is found to be negligible for all vibrational levels and at all N_2 fractions and power densities investigated, because of the faster VV rates.

5. CONCLUSIONS

We presented a 0D chemical kinetics model for a CO_2/N_2 microwave plasma, with special emphasis on the vibrational levels of both CO_2 and N_2. For CO_2, 4 effective symmetric mode energy levels as well as 21 asymmetric mode levels, i.e., up to the dissociation limit, are taken into account, whereas for N_2, 14 vibrational levels are included. In addition, also 10 CO vibrational levels and 4 O_2 vibrational levels are considered. A detailed description of the vibrational processes, including vibrational excitation, VT and VV relaxation, and chemical reactions of the vibrational levels, is included.

The model is used to calculate the CO_2 and N_2 conversion as well as the energy efficiency for CO_2 conversion at a gas pressure of 2660 Pa and a gas inlet temperature of 300 K for three different values of power density in the range of 30−80 W/cm^3 and for N_2 fractions in the gas mixture ranging from 0 until 90%. The absolute CO_2 conversion is in the order of 10−80%, rising with power density and with N_2 fraction. This indicates that N_2 has a beneficial effect on the CO_2 conversion. The effective CO_2 conversion, on the other hand, remains constant or drops slightly upon rising N_2 fraction, as there is less CO_2 present in the gas mixture.

The absolute N_2 conversion is calculated to be in the order of 2−20% at the conditions under study. It remains more or less constant or rises slightly upon increasing N_2 fraction, except in the higher range of N_2 fractions, where it clearly drops. The reason is that many reactive N-compounds are formed, which again give rise to the formation of N_2 and thereby limit the net N_2 conversion. The effective N_2 conversion generally increases because there is more N_2 initially present, except again at the highest N_2 fractions, for the reason explained above.

The energy efficiency is in the order of 8−15% and remains more or less constant when varying the N_2 fraction, except in the low or high range of N_2 fractions. At low N_2 fractions, the energy efficiency is the highest for the higher power density, whereas at high N_2 fractions, the opposite behavior is observed, i.e., the energy efficiency is highest for the lowest power density.

The calculated CO_2 and N_2 conversions and the energy efficiencies are compared with experimental data, measured for exactly the same conditions, and generally, agreements within 23% and 33% are obtained, indicating that the model can already qualitatively describe the underlying plasma physics and chemistry in CO_2/N_2 microwave discharges.

To explain the observed trends, we have analyzed the destruction and formation processes of both CO_2 and N_2 as well as their vibrational distribution functions. The major destruction process for CO_2 is dissociation of vibrationally excited CO_2 upon collision with any molecule or atom in the plasma, especially at the higher power densities. At the lowest power density investigated and low N_2 fractions, electron impact dissociation from CO_2, both in the ground state and vibrationally excited levels, are more important. Because dissociation from the ground state requires a significant amount of energy, this explains the somewhat lower energy efficiency obtained at the lowest power density and low N_2 fractions. CO_2 will also be formed again, e.g., by reactions between reactive N-compounds (NCO and NO) at the highest N_2 fractions and by reactions with ions or with CO and O^- at lower N_2 fractions, but these processes are of minor importance, as the total formation rate of CO_2 is 2 orders of magnitude lower than the total destruction rate.

N_2 is almost exclusively destroyed by the reaction between vibrationally excited N_2 molecules and O atoms, yielding the formation of N and NO, at all conditions investigated. However, the reverse process, i.e., the reaction of N with NO (or with NO_2) yielding O atoms (or O_2 molecules) and N_2 molecules, is also an important formation mechanism. In contrast to CO_2, the total formation rate of N_2 is typically only a factor of 1.1−3 lower than the total destruction rate, explaining the lower conversion compared to that of CO_2.

Finally, the VDFs of CO_2 and N_2 are calculated. The VDFs of N_2 are virtually equal to each other at all N_2 fractions and power densities investigated; they drop slightly upon increasing level number for the levels 1−11, but the populations of the higher levels are much lower. The calculated VDFs of CO_2 illustrate that the vibrational levels of CO_2 are important at all power densities investigated, especially at high N_2 fractions. As a result, the importance of the vibrationally excited CO_2 levels is also equally important for the CO_2 destruction at these high

DOI: 10.1021/acs.jpcc.5b01466
J. Phys. Chem. C 2015, 119, 12815−12828

N_2 fractions, and this explains why the power density of 30 W/cm^3 will yield a higher energy efficiency. Our calculations reveal that the lower CO_2 vibrational levels are mainly populated by electron impact vibrational excitation at low N_2 fractions, but at high N_2 fractions, VV relaxation with N_2 becomes increasingly important. Subsequently, VV relaxation with CO and CO_2 will (partially) convert these lower levels into the higher vibrational levels, which are essential for energy-efficient CO_2 splitting. This illustrates the important role of N_2 in populating the CO_2 vibrational levels and explains the higher CO_2 conversion upon addition of N_2. In general, we can conclude that both the CO_2 and N_2 vibrational levels play a very important role in the (energy-efficient) CO_2 conversion.

■ ASSOCIATED CONTENT

Supporting Information

The extra coupling reactions between CO_2 and N_2, as well as the corresponding rate coefficients; a sensitivity analysis of the most important reactions; and validation of the 0D approach. The Supporting Information is available free of charge on the ACS Publications website at DOI: 10.1021/acs.jpcc.5b01466.

■ AUTHOR INFORMATION

Corresponding Authors

*E-mail: stijn.heijkers@uantwerpen.be.
*E-mail: annemie.bogaerts@uantwerpen.be.

Notes

The authors declare no competing financial interest.

■ ACKNOWLEDGMENTS

The authors acknowledge financial support from the IAP/7 (Interuniversity Attraction Pole) program "PSI-Physical Chemistry of Plasma-Surface Interactions" by the Belgian Federal Office for Science Policy (BELSPO), from the Francqui Research Foundation, and from the Fund for Scientific Research Flanders (FWO). N.B. is a postdoctoral researcher of the Belgian National Fund for Scientific Research (FNRS). The calculations were performed using the Turing HPC infrastructure at the CalcUA core facility of the Universiteit Antwerpen, a division of the Flemish Supercomputer Center VSC, funded by the Hercules Foundation, the Flemish Government (department EWI) and the Universiteit Antwerpen.

■ REFERENCES

(1) Fridman, A. *Plasma Chemistry*; Cambridge University Press: New York, 2008.
(2) Gutsol, A.; Rabinovich, A.; Fridman, A. Combustion-Assisted Plasma in Fuel Conversion. *J. Phys. D: Appl. Phys.* **2011**, *44*, 274001.
(3) Paulussen, S.; Verheyde, B.; Tu, X.; De Bie, C.; Martens, T.; Petrovic, D.; Bogaerts, A.; Sels, B. Conversion of Carbon Dioxide to Value-Added Chemicals in Atmospheric Pressure Dielectric Barrier Discharges. *Plasma Sources Sci. Technol.* **2010**, *19*, 034015.
(4) Indarto, A.; Yang, D. R.; Choi, J. W.; Lee, H.; Song, H. K. Gliding Arc Plasma Processing of CO_2 Conversion. *J. Hazard. Mater.* **2007**, *146*, 309−315.
(5) Nunnally, T.; Gutsol, K.; Rabinovich, A.; Fridman, A; Gutsol, A; Kemoun, A. Dissociation of CO_2 in a Low Current Gliding Arc Plasmatron. *J. Phys. D: Appl. Phys.* **2011**, *44*, 274009.
(6) Britun, N.; Godfroid, T.; Snyders, R. Time-Resolved Study of Pulsed Ar−N_2 and Ar−N_2−H_2 Microwave Surfaguide Discharges Using Optical Emission Spectroscopy. *Plasma Sources Sci. Technol.* **2012**, *21*, 035007.
(7) Silva, T.; Britun, N.; Godfroid, T.; Snyders, R. Optical Characterization of a Microwave Pulsed Discharge Used for Dissociation of CO_2. *Plasma Sources Sci. Technol.* **2014**, *23*, 025009.
(8) Maya, L. Plasma-Assisted Reduction of Carbon Dioxide in the Gas Phase. *J. Vac. Sci. Technol., A* **2000**, *18*, 285.
(9) Spencer, L. F.; Gallimore, A. D. CO_2 Dissociation in an Atmospheric Pressure Plasma/Catalyst System: A Study of Efficiency. *Plasma Sources Sci. Technol.* **2013**, *22*, 015019.
(10) Ihara, T.; Ouro, T.; Ochiai, T.; Kiboku, M.; Iriyama, Y. Formation of Methanol by Microwave-Plasma Reduction of CO_2 with H_2O. *Bull. Chem. Soc. Jpn.* **1996**, *69*, 241−244.
(11) Zhang, J. Q.; Yang, Y. J.; Zhang, J. S.; Liu, Q. Study on the Conversion of CH_4 and CO_2 Using a Pulsed Microwave Plasma under Atmospheric Pressure. *Acta Chim. Sin. (Chin. Ed.)* **2002**, *60*, 1973−1980.
(12) Fidalgo, B.; Domínguez, A.; Pis, J. J.; Menéndez, J. A. Microwave-Assisted Dry Reforming of Methane. *Int. J. Hydrogen Energy* **2008**, *33*, 4337−4344.
(13) Rusanov, V. D.; Fridman, A. A.; Sholin, G. V. The Physics of a Chemically Active Plasma with Nonequilibrium Vibrational Excitation of Molecules. *Uspekhi Fiz. Nauk* **1981**, *134*, 185.
(14) Asisov, R. I.; Fridman, A. A.; Givotov, V. K.; Krasheninnikov, E. G.; Petrushev, B. I.; Potapkin, B. V.; Rusanov, V. D.; Krotov, M. F.; Kurchatov, I. V. *5th Int. Symp. on Plasma Chemistry (Edinburgh, UK)*; 1981; Vol. 2.
(15) Zhang, K.; Eliasson, B.; Kogelschatz, U. Direct Conversion of Greenhouse Gases to Synthesis Gas and C_4 Hydrocarbons over Zeolite HY Promoted by a Dielectric-Barrier Discharge. *Ind. Eng. Chem. Res.* **2002**, *41*, 1462−1468.
(16) Wang, Q.; Yan, B. H.; Jin, Y.; Cheng, Y. Dry Reforming of Methane in a Dielectric Barrier Discharge Reactor with Ni/Al_2O_3 Catalyst: Interaction of Catalyst and Plasma. *Energy Fuels* **2009**, *23*, 4196−4201.
(17) Tu, X.; Gallon, H. J.; Twigg, M. V.; Gorry, P. A.; Whitehead, J. C. Dry Reforming of Methane over a Ni/Al_2O_3 Catalyst in a Coaxial Dielectric Barrier Discharge Reactor. *J. Phys. D: Appl. Phys.* **2011**, *44*, 274007.
(18) Scarduelli, G.; Guella, G.; Ascenzi, D.; Tosi, P. Synthesis of Liquid Organic Compounds from CH_4 and CO_2 in a Dielectric Barrier Discharge Operating at Atmospheric Pressure. *Plasma Processes Polym.* **2011**, *8*, 25−31.
(19) Snoeckx, R.; Aerts, R.; Tu, X.; Bogaerts, A. Plasma-Based Dry Reforming: A Computational Study Ranging from the Nanoseconds to Seconds Time Scale. *J. Phys. Chem. C* **2013**, *117* (4), 4957−4970.
(20) Eliasson, B.; Kogelschatz, U.; Xue, B.; Zhou, L. 99/01083 Hydrogenation of Carbon Dioxide to Methanol with a Discharge-Activated Catalyst. *Fuel Energy Abstr.* **1999**, *40*, 112.
(21) Kano, M.; Satoh, G.; Iizuka, S. Reforming of Carbon Dioxide to Methane and Methanol by Electric Impulse Low-Pressure Discharge with Hydrogen. *Plasma Chem. Plasma Process.* **2012**, *32*, 177−185.
(22) Pinhão, N. R.; Janeco, A.; Branco, J. B. Influence of Helium on the Conversion of Methane and Carbon Dioxide in a Dielectric Barrier Discharge. *Plasma Chem. Plasma Process.* **2011**, *31*, 427−439.
(23) Tsuji, M.; Tanoue, T.; Nakano, K.; Nishimura, Y. Decomposition of CO_2 into CO and O in a Microwave-Excited Discharge Flow of CO_2/He or CO_2/Ar Mixtures. *Chem. Lett.* **2001**, *1*, 22−23.
(24) Savinov, S. Y.; Lee, H.; Song, H. K.; Na, B.-K. The Decomposition of CO_2 in Glow Discharge. *Korean J. Chem. Eng.* **2002**, *19*, 564−566.
(25) Nighan, W. L. Electron Energy Distributions and Collision Rates in Electrically Excited N_2, CO, and CO_2. *Phys. Rev. A* **1970**, *2*, 1989−2000.
(26) Cenian, A.; Chernukho, A.; Borodin, V. Modeling of Plasma-Chemical Reactions in Gas Mixture of CO_2 Lasers. II. Theoretical Model and Its Verification. *Contrib. to Plasma Phys.* **1995**, *35*, 273−296.
(27) Guerra, V.; Loureiro, J. Non-Equilibrium Coupled Kinetics in Stationary N_2-O_2 Discharges. *J. Phys. D: Appl. Phys.* **1995**, *28*, 1903.

DOI: 10.1021/acs.jpcc.5b01466
J. Phys. Chem. C 2015, 119, 12815−12828

(28) Guerra, V.; Tatarova, E.; Dias, F. M.; Ferreira, C. M. On the Self-Consistent Modeling of a Traveling Wave Sustained Nitrogen Discharge. *J. Appl. Phys.* **2002**, *91*, 2648−2661.
(29) Capitelli, M.; Colonna, G.; Ammando, G. D.; Laporta, V. Nonequilibrium Dissociation Mechanisms in Low Temperature Nitrogen and Carbon Monoxide Plasmas. *Chem. Phys.* **2014**, *438*, 31−36.
(30) Kozák, T.; Bogaerts, A. Splitting of CO_2 by Vibrational Excitation in Non-Equilibrium Plasmas: A Reaction Kinetics Model. *Plasma Sources Sci. Technol.* **2014**, *23*, 045004.
(31) Kozak, T.; Bogaerts, A. Evaluation of the Energy Efficiency of CO_2 Conversion in Microwave Discharges Using a Reaction Kinetics Model. *Plasma Sources Sci. Technol.* **2015**, *015024*.
(32) Pancheshnyi, S.; Eismann, B.; Hagelaar, G. J. M.; Pitchford, L. C. *ZDPlasKin: A New Tool for Plasmachemical Simulations*, 2008.
(33) Hagelaar, G. J. M.; Pitchford, L. C. Solving the Boltzmann Equation to Obtain Electron Transport Coefficients and Rate Coefficients for Fluid Models. *Plasma Sources Sci. Technol.* **2005**, *14*, 722−733.
(34) White, R. D.; Robson, R. E.; Schmidt, B.; Morrison, M. A. Is the Classical Two-Term Approximation of Electron Kinetic Theory Satisfactory for Swarms and Plasmas? *J. Phys. D: Appl. Phys.* **2003**, *36*, 3125−3131.
(35) Loffhagen, D.; Winkler, R.; Braglia, G. L. Two-Term and Multi-Term Approximation of the Nonstationary Electron Velocity Distribution in an Electric Field in a Gas. *Plasma Chem. Plasma Process.* **1996**, *16*, 287−300.
(36) Pitchford, L. C.; Phelps, A. V. Comparative Calculations of Electron-Swarm Properties in N_2 at Moderate E/N Values. *Phys. Rev. A* **1982**, *25*, 540−554.
(37) Aleksandrov, N. Kinetics of Low-Temperature Plasmas for Plasma-Assisted Combustion and Aerodynamics. *Plasma Sources Sci. Technol.* **2014**, *23*, 015017.
(38) Lowke, J. J.; Phelps, A. V.; Irwin, B. W. Predicted Electron Transport Coefficients and Operating Characteristics of CO_2−N_2−He Laser Mixtures. *J. Appl. Phys.* **1973**, *44*, 4664−4671.
(39) Westley, F. *Table of Recommended Rate Constants for Chemical Reactions Occurring in Combustion*; NSRDS-NBS 67; National Bureau of Standards, U.S. Government Printing Office: Washington, DC, 1980115
(40) Baulch, D. L.; Cobos, C. J.; Cox, R. A.; Esser, C.; Frank, P.; Just, T.; Kerr, J. A.; Pilling, M. J.; Troe, J.; Walker, R. W.; et al. Evaluated Kinetic Data for Combustion Modelling. *J. Phys. Chem. Ref. Data* **1992**, *21*, 411.
(41) Dünkel, L. Topics in Current Physics: Nonequilibrium Vibrational Kinetics. In *Topics in Current Physics*; Capitelli, M., Ed.; Springer: Berlin, 1991; Vol. *39*, p 344.
(42) Treanor, C. E. Vibrational Relaxation of Anharmonic Oscillators with Exchange-Dominated Collisions. *J. Chem. Phys.* **1968**, *48*, 1798−1807.
(43) Blauer, J. A.; Nickerson, G. R. *A Survey of Vibrational Relaxation Rate Data For Processes Important To CO_2-N_2-H_2O Infrared Plume Radiation*; AFRPL-TR-73-57; Air Force Rocket Propulsion Laboratory, Director of Science and Technology, Air Force Systems Command: Edwards, CA, 1973.
(44) Schwartz, R. N.; Slawsky, Z. I.; Herzfeld, K. F. Calculation of Vibrational Relaxation Times in Gases. *J. Chem. Phys.* **1952**, *20*, 1591.
(45) Adamovich, I. V.; MacHeret, S. O.; Rich, J. W.; Treanor, C. E. Vibrational Energy Transfer Rates Using a Forced Harmonic Oscillator Model. *J. Thermophys. Heat Transfer* **1998**, *12*, 57−65.
(46) Adamovich, I. V.; Rich, J. W. Three-Dimensional Non-perturbative Analytic Model of Vibrational Energy Transfer in Atom-Molecule Collisions. *J. Chem. Phys.* **1998**, *109*, 7711−7724.
(47) Da Silva, M. L.; Guerra, V.; Loureiro, J. State-Resolved Dissociation Rates for Extremely Nonequilibrium Atmospheric Entries. *J. Thermophys. Heat Transfer* **2007**, *21*, 40−49.
(48) Capitelli, M.; Ferreira, C. M.; Gordiets, B. F.; Osipov, A. I. *Plasma Kinetics in Atmospheric Gases*; Springer: Berlin, 2000.
(49) Odrobina, I.; Kúdela, J.; Kando, M. Characteristics of the Planar Plasma Source Sustained by Microwave Power. *Plasma Sources Sci. Technol.* **1999**, *7*, 238−243.
(50) Kiss'ovski, Z.; Brockhaus, A.; Korzec, D.; Kytzia, S.; Engemann, J. Plasma Parameters of an Oxygen Microwave Discharge Obtained by Probe Diagnostics: II. Radial Distributions. *Plasma Sources Sci. Technol.* **2007**, *16*, 523−528.
(51) Kato, I.; Hara, S.; Wakana, S. Analysis of Radial Distribution of Plasma Parameters in a Coaxial-Line Microwave Discharge Tube. *J. Appl. Phys.* **1983**, *54*, 4883.
(52) Hassouni, K.; Gicquel, A.; Grotjohn, T. A. Self-Consistent Microwave Field and Plasma Discharge Simulations for a Moderate Pressure Hydrogen Discharge Reactor. *25th Anniversary, IEEE Conference Record - Abstracts. 1998 IEEE International Conference on Plasma Science*, 1998; Cat. No. 98CH36221, *134*.
(53) Schlüter, H.; Shivarova, A. Travelling-Wave-Sustained Discharges. *Phys. Rep.* **2007**, *443*, 121−255.

DOI: 10.1021/acs.jpcc.5b01466
J. Phys. Chem. C 2015, 119, 12815−12828